Geophysical Journal International

Geophys. J. Int. (2026) **246,** 1–13
Advance Access publication 2026 April 23
Research paper

https://doi.org/10.1093/gji/ggag155

Analysis of the 2019 M_w 6.4 Durrës, Albania, aftershock sequence: basement involved thrusting at the eastern Adriatic plate margin

Vincent van der Heiden [1,†] Bernd Schurr [2] Jack Woollam,[1] Edmond Dushi [3] Frederik Tilmann [2,4] and Andreas Rietbrock [1]

[1]*Geophysical Institute, Karlsruhe Institute of Technology (KIT), Hertzstrasse 16, 76187 Karlsruhe, Germany*
[2]*Helmholtz Centre for Geosciences (GFZ), Telegrafenberg, 14473 Potsdam, Germany. E-mail: schurr@gfz.de*
[3]*Department of Seismology, Institute of Geosciences (IGEO), Polytechnic University, Don Bosko 60, 1024 Tirana, Albania*
[4]*Institute for Geological Sciences, Freie Universität Berlin (FU), Malteserstr. 74-100, 12249 Berlin, Germany*

Accepted 2026 April 12. Received 2026 April 8; in original form 2025 September 30

SUMMARY

The 2019 *M* 6.4 Durrës earthquake in Albania caused severe loss of life and economic damage, highlighting the seismic hazard along the Adriatic–European plate boundary. This study provides the first high-resolution analysis of the aftershock sequence based on data from a dense local seismic network deployed three weeks after the mainshock. Using machine-learning detection and phase-picking tools, we identified 19 152 aftershocks (Ml − 1.8 to 4.6; Mc ≈ 1) over a nine-month period. Based on a newly derived 1-D velocity model with station corrections, accounting for large vertical and lateral velocity variations, we relocated the events applying cross-correlation based differential traveltimes and the double-difference algorithm. The refined seismicity images clearly reveal several subparallel ∼30° NE-dipping blind fault structures; the most prominent one, between 12 and 18 km depth, probably hosted the Durrës mainshock. The blind thrust faults lie beneath thick sediments and cut through a carbonate platform and into the Adriatic basement, indicating thick-skinned deformation. Our observations may be interpreted as incipient large-scale slicing and underplating of subducted Adriatic crust. Additional shallow seismicity within a duplex structure in the hanging wall points is relevant for seismic hazard, as even a relatively moderate earthquake occurring close to the surface could cause significant damage.

Key words: Earthquake source observations; Earthquake hazards; Continental margins: convergent; Dynamics and mechanics of faulting; Dynamics: seismotectonics.

INTRODUCTION

On 2019 November 26, Albania was struck by a *M* 6.4 earthquake 10 km north of the Adriatic port Durrës and 30 km away from the capital city of Tirana, claiming 51 lives and leaving 2000 citizens seriously injured, making it the world-wide deadliest seismic event of the year 2019. Additionally, it caused about 1 billion Euro damage, or 7.5 per cent of Albania's 2018 gross domestic product (F. Freddi *et al*. 2021).

Such events are not uncommon to the western Balkan region where compressional stresses build up along the plate boundary between the Adriatic microplate and the Eurasian continent (Fig. 1). Particularly the eastern Adriatic margin along the Dinarides and Albanides/Hellenides fold and thrust belts has seen numerous devastating earthquakes. In 1667, an earthquake with intensity IX–X destroyed the city of Ragusa, now Dubrovnik, with long-lasting consequences for the region (S. Markušić *et al*. 2017). More recently, a shallow thrust earthquake with *M* 7.1 occurred in 1979 near the coastal city of Bar in Montenegro, roughly halfway between Dubrovnik and Durrës, (C. Benetatos & A. Kiratzi 2006), making it one of the largest events within Europe in instrumental times. Durrës itself, an important port all the way back to the Greek and Roman empires, was struck repeatedly by earthquakes with intensities ≥IX in, for example, 346, ∼521, 1270 and in a sequence in 1869–1870 (E. Vittori et al. 2021).

The thrusts of both the 1979 Montenegro and the recent Durrës earthquake were blind and relatively little is known about their source fault structures. The Durrës earthquake was part of a sequence which started two months prior with two foreshocks of *M* 5.6 and *M* 5.1 south of the mainshock (Fig. 2). Despite being one of the seismically most active regions in Europe, seismic monitoring in Albania and surroundings was relatively sparse at the time of the earthquake. The sequence was recorded by only one nearfield station (MN.TIR) within ∼30 km epicentral distance. Accordingly, reported hypocentre locations of the foreshocks, mainshock and

[†]Now at: Utrecht University, Princetonlaan 4, 3584 CB Utrecht

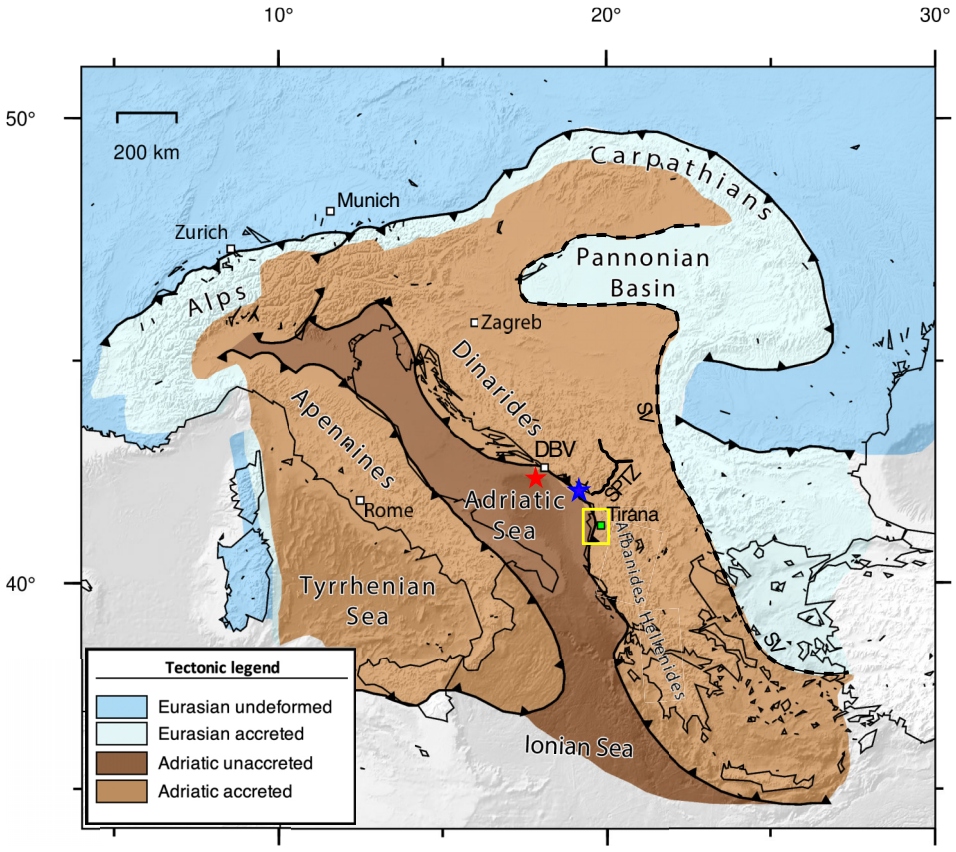

Figure 1. Simplified geologic map of the central Mediterranean region. The yellow rectangle marks the region where the *M* 6.4 Durrës earthquake took place near the Albanian capital Tirana. Blue star marks the approximate location of the 1667 Ragusa/Dubrovnik earthquake, the red star the approximate location of the 1979 M7 Bar, Montenegro earthquake. DBV—Dubrovnik, SPTZ—Shkodra-Pec transfer zone, SV—Sava suture. Major faults and plate boundaries from M.R. Handy *et al.* (2015).

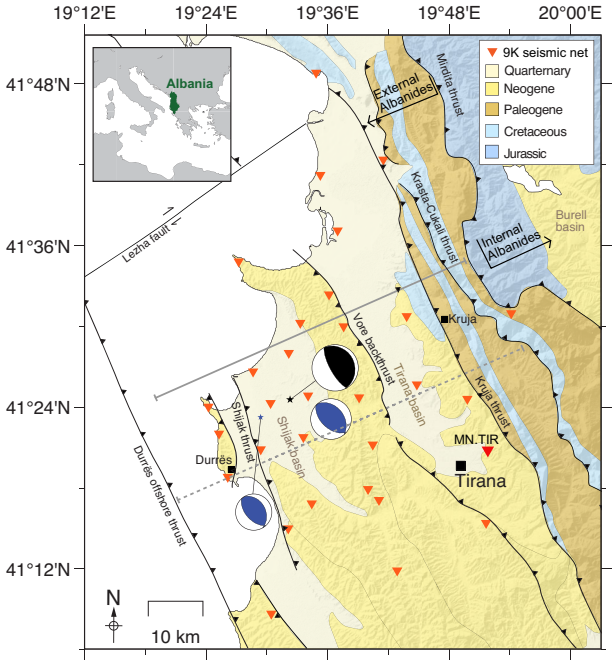

Figure 2. Tectonic and geological setting of the Durrës region, Albania. The 30 stations of the temporary AlbACa (network code 9 K, 2019–2020) seismic network are plotted with inverted triangles. Geology is drawn after A. Xhomo *et al.* (2002). Black beachball depicts the double couple solution for the 2019 November 26 Durrës mainshock reported by GEOFON (see Table 1), blue beachballs are the two M5 + foreshocks from September 2019. The dashed line shows the location of the structural cross section published by F. Roure *et al.* (2004). The parallel solid line indicates the profile depicted in Fig. 10. MN.TIR is the permanent MEDNET station Tirana.

Table 1. Source parameters of the 2019 Durrës mainshock reported by different agencies; accessed through Euro-Mediterranean Seismological Centre (EMSC).

Agency	Nodal plane 1			Nodal plane 2			Centroid			
	Strike (°)	Rake (°)	Dip (°)	Strike (°)	Rake (°)	Dip (°)	Longitude (°)	Latitude (°)	Depth (km)	M_w
GFZ	150	88	72	335	94	18	19.54	41.41	26	6.4
GCMT	145	79	68	351	114	25	19.45	41.39	24.1	6.4
NEIC	156	89	63	338	92	27	19.53	41.51	19.5	6.4
IPGP	151	81	72	357	115	20	19.48	41.42	24	6.5
INGV	134	84	82	350	126	10	19.52	41.40	21	6.2
AUTH	150	109	49	303	69	44	19.44	41.45	6	6.1
CPPT	168	104	69	312	57	25	19.40	41.40	15	6.4

aftershocks show significant variation, highlighting their uncertainty (Table 1). Depth estimates in particular varied between 6 and 26 km for the mainshock. Although published moment tensors indicate consistently thrusting on NNW trending planes, the variation of strikes (303°–357°) and dips (10°–44°) of the east dipping plane leave enough ambiguity to associate the earthquake with any mapped or unmapped structure.

The earthquake was well recorded by the Sentinel 1 satellite, prompting several source models based on interferometric synthetic aperture radar (InSAR) derived surface deformation (A. Ganas *et al.* 2020; M. Govorčin *et al.* 2020; H. Panuntun 2021; E. Vittori *et al.* 2021; G. Pezzo *et al.* 2022; K. Matraku *et al.* 2023). However, InSAR gives also only limited constraints on depth and fault dip. Moreover, even the choice of the two possible nodal planes is ambiguous. While most studies chose the north–east-dipping plane, mostly on geological grounds, some (M. Govorčin *et al.* 2020; G. Pezzo *et al.* 2022) preferred rupture on a steeply south–west-dipping backthrust.

In this study, we use data from a dense local network deployed three weeks after the mainshock to obtain high-resolution aftershock locations that precisely illuminate the activated fault structures. Our results provide new insights into the mode of deformation at the leading edge of the Adriatic–European plate boundary zone, an important yet understudied seismogenic structure in Europe.

TECTONIC SETTING

The western Adriatic margin is formed by collision between the Adriatic microplate and the European continent, building the Dinarides and Hellenides fold and thrust belts. Continental collision initiated during Late Jurassic and Early Cretaceous when the northernmost part of the Neotethys ocean was consumed and the so-called Vardar ophiolites obducted. Today the Sava Suture zone traces the boundary between Adriatic and European crust (Fig. 1).

The term Albanides is often used for the northernmost part of the Hellenides situated in Albania, although they form a single geological structure. Along strike, the Dinarides and Hellenides are separated by the Shkodra-Pec transfer zone (SPTZ), along which the Vardar ophiolite belt is dextrally offset by ∼80 km. It coincides also with a 30° clockwise kink between the two belt segments. The oldest ophiolitic and crystalline rocks are now forming the internal Dinarides/Hellenides. The collision is continuing until today and the orogen has been growing outward by scraping off and accreting Adriatic nappes on to the margin, forming the external Dinarides/Hellenides. The amount of shortening increases southward from about 80 km in the southernmost Dinarides to twice this amount in the southern Hellenides (M.R. Handy *et al.* 2019). Todays geodetically measured shortening rates follow a similar trend (F. Jouanne *et al.* 2012). This gradient has been attributed to oroclinal bending. Paleomagnetic data indicate up to 50° clockwise rotation of the Hellenides since the Eocene–Oligocene time. Instantaneous clockwise rotation of comparable rate is measured today geodetically with a pivot roughly near the SPTZ (N. D'Agostino *et al.* 2020). The SPTZ is also the northernmost extent of southward increasing orogen-parallel extension along the internal Hellenides. The drivers of rotation and extension have been attributed to either buoyancy forces due to topographic and rheological gradients (e.g. N. D'Agostino et al. 2020) or to slab roll-back of the subducted Adriatic and Ionian slabs and accompanying trench retreat (e.g. M.R. Handy *et al.* 2019). Today, shortening across the eastern Adriatic margin occurs with a rate of ∼4 mm a^{-1} in our study region. The Durrës earthquake occurred at the outermost deformation front of the external Albanides and its thrust mechanism is evidence for active shortening.

The external northern Albanides in our study region consist of Triassic to Eocene carbonites and Oligocene to Pliocene siliciclastic deposits, making up three major tectonics zones, from east to west called the Krasta–Cukali, Kruja and Ionian zone, delimited by the Mirdit, Krasta–Cukali and Kruja thrusts (Fig. 2). Geology of the Krasta–Cukali zone is characterized by pelagic basin rocks of Jurassic to Paleogene age. The Kruja zone consists of overthrusted shelf limestone nappes of Late Cretaceous age. The Ionian zone, also called the Periadriatic Depression, represents the Mesozoic to Cenozoic passive continental margin of Apulia/Adria, dominated by Holocene and Neogene sediments above a carbonate platform (S. Teloni *et al.* 2020; E. Vittori *et al.* 2021). The three external Albanides zones are lying on top of an Early Triassic crystalline basement. Several studies have speculated whether the Durrës rupture took place along a Triassic evaporite detachment layer potentially present atop the basement (S. Teloni *et al.* 2020; E. Vittori *et al.* 2021; K. Matraku *et al.* 2023). The Vore backthrust, which separates the Tirana and Shijak basins, as well as the Shijak thrust are thought to be passive roof thrusts cutting through the siliciclastic and carbonate deposits of the Periadriatic Depression (Fig. 2).

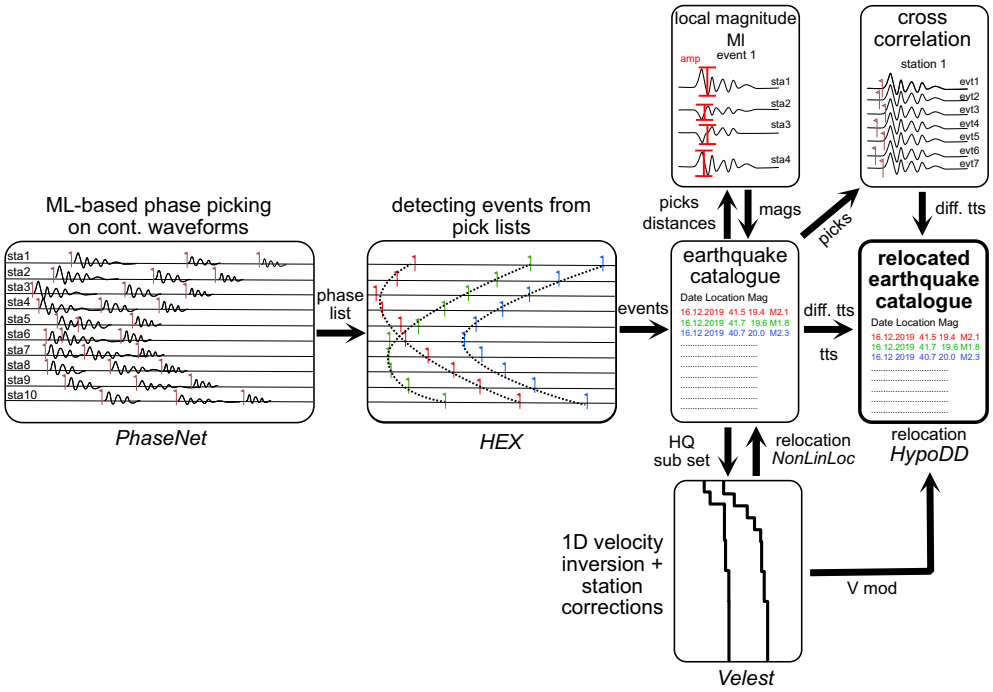

Figure 3. Flowchart of the different processing steps that lead to the final earthquake catalogue. The processing scheme was largely automated, enabling processing of a large number of events. Specific computer programs used are written in italics and explained and referenced in the text. tts—traveltimes, HQ—high-quality, diff—differential.

DATA

In order to observe the aftershock sequence in detail and to resolve the source fault structures, the Helmholtz Center for Geosciences (GFZ) and the Karlsruhe Institute of Technology (KIT) in cooperation with the Institute of Geosciences (IGEO) of the Polytechnic University of Tirana, Albania, installed the AlbACa (Albanian Earthquake Aftershock Campaign) seismic network approximately three weeks after the mainshock in the epicentral region (Fig. 2). The network consisted of 20 3-component geophones with 4.5 Hz natural frequency and 10 3-component short-period seismometers with 1 Hz natural frequency recording at 100 Hz sampling rate. The network covered a region of ∼70 km × 40 km with 5–10 km interstation separation. Recording lasted from mid-December 2019 to September 2020 (B. Schurr *et al*. 2020).

AFTERSHOCK CATALOGUE PRODUCTION

We employed a mostly automated processing scheme, starting from the continuous three-component waveforms and resulting in a final high-resolution earthquake catalogue located in a tailor-made velocity model (Fig. 3). The specific steps are explained in the following subsections.

MACHINE LEARNING-BASED EVENT DETECTION AND PHASE PICKING

Aftershock sequences typically have very high-seismicity rates, making their analysis with traditional means, that is, visual inspection and phase-picking, cumbersome, with the result that often only subsets of data are analysed. In recent years, Machine Learning (ML) based methods have been developed and successfully applied to take over this task, making the processing of very large data sets possible (e.g. Y.J. Tan *et al*. 2021). We applied the well-established PhaseNet (W. Zhu & G.C. Beroza 2019) neural network for phase detection and arrival time picking to the nine months of continuous, unfiltered 3-component data. We used PhaseNet's default value of 0.3 for the probability cut-off to create candidate picks. To form events from the phase lists the Hyperbolic Event eXtractor (HEX; J. Woollam *et al*. 2020) was employed. HEX automatically associates seismic phase picks by robustly fitting hyperbolic traveltime curves to identify and group arrivals from the same underlying seismic event. J. Woollam *et al*. (2022) did carefully tested the performance of different algorithms for picking and associating for a two-week subset of our data, which was also manually picked. They found that ML-based picks are consistent with manual picks, with bias that is no larger than that between different analysts. Data fit for locations was comparable to that of the analysts' picks but the increased number of picks per event for the ML pickers decreased hypocentral errors.

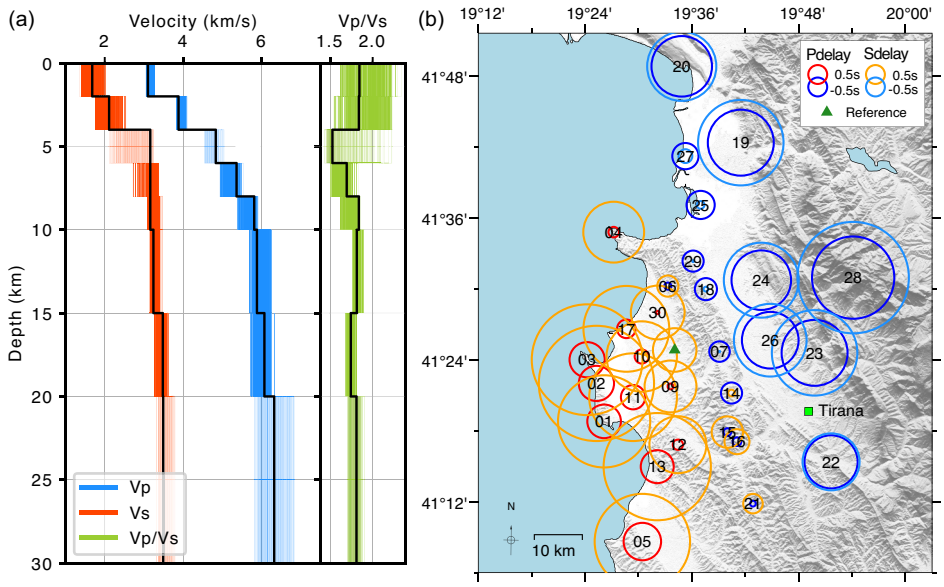

Figure 4. (a) The best V_p and V_s output model (thick black lines) and the 433 best out of 1000 output models (coloured thin lines), with the corresponding V_p/V_s ratio (see Table S1 in the Supplementary Information). (b) Spatial distribution of station correction terms for *P*- (red, dark blue) and *S*-phase (orange, light blue) observations (see Table S2 in the Supplementary Information). Station numbers are indicated. The reference station is marked by a green triangle.

Applying these procedures, 19 152 events were detected comprising 239 418 *P*- and 188 838 *S*-phase arrivals. For all detections, probabilistic hypocentres were calculated with the NonLinLoc software (NLL; A. Lomax *et al.* 2000), using a published velocity model for Albania (R. Ormeni, 2011; Fig. S1, Supplementary Information). Counter-intuitively, the events located with this velocity model appear to dip to the SW (Fig. S1, Supplementary Information). This pattern will reverse, as we will see in the next chapter with a velocity model derived specifically for the region. The NLL method provides posterior phase weights to effectively remove phase arrival outliers in the ML-based aftershock catalogue. Any phase with a NLL posterior phase weight lower than 0.4 was removed from the data set for the final locations.

ONE-DIMENSIONAL VELOCITY MODEL

Although our network has a small footprint, it covers a sequence of uplifted ridges and intervening deep sedimentary basins (Fig. 2), which are expected to produce strong velocity contrasts. We therefore inverted for a new 1-D velocity model and a set of station corrections representative for our data by applying the Velest code (E. Kissling et al. 1994). To avoid overrepresenting depth ranges with high seismicity in the inversion, we applied depth binning by dividing the 0–30 km depth range into 1-km intervals. From each depth bin, the highest-quality events were selected up to a fixed maximum that increases with depth, from 15 events in the shallowest bins to 30 events at 30 km depth, ensuring a well-balanced depth distribution. In this way, we selected a subset of the best located ($\geq$15 *P*, $\geq$10 *S* picks, azimuthal gap $\leq 170^{\circ}$) $\sim$500 events for the velocity inversion. Our starting model was guided by an onshore–offshore 2-D seismic wide-angle experiment just north of the study region (Anke Dannowski, personal communication). This model was perturbed 1000 times within sensible limits to mitigate ending up in a local misfit minimum. The best 5 per cent output models (433 models) are shown in Fig. 4, and we can use their scatter as an indication of uncertainty or non-uniqueness of the solution. Inversion of the single best model shows a reduction in the traveltime rms of $-$55.2 per cent, from 0.494 to 0.221 s; the resulting model can be found in Table S1 (Supplementary Information).

Velocities in the uppermost two layers, up to 4 km depth are typical for sedimentary layers; the V_p/V_s ratio is 1.8 but with large uncertainty (allowable range 1.6–2.3), driven by large uncertainty in V_s. Velocities then increase on steep gradient up to about 10 km depth, with V_p/V_s ratios somewhat unstable, but generally lower than in the top 4 km. V_p/V_s remains nearly constant at around 1.8 for the deeper section of the model, where V_s and V_p increase very slowly to $V_s = 4.0$ km s^{-1} and $V_p = 7.3$ km s^{-1} at 30 km depth, the largest depth our local earthquake catalogue allows us to resolve.

P-phase station correction terms relative to reference station AB08 lie between $-$2.2 s and 1 s and *S*-phase station correction terms between $-$3 s and +3 s (Fig. 4b). Their well-defined spatial pattern correlates with the surface geology. The positive station correction terms in the SW (= slower velocities) correspond to Neogene and Paleogene deposits and the negative station correction terms in the NE (= faster velocities) correspond to carbonates and Jurassic ophiolites in the internal Albanides (E. Vittori *et al.* 2021). The systematic variations and large amplitudes of the corrections point to large velocity variations and emphasize the importance of them being taken into account in the location procedure.

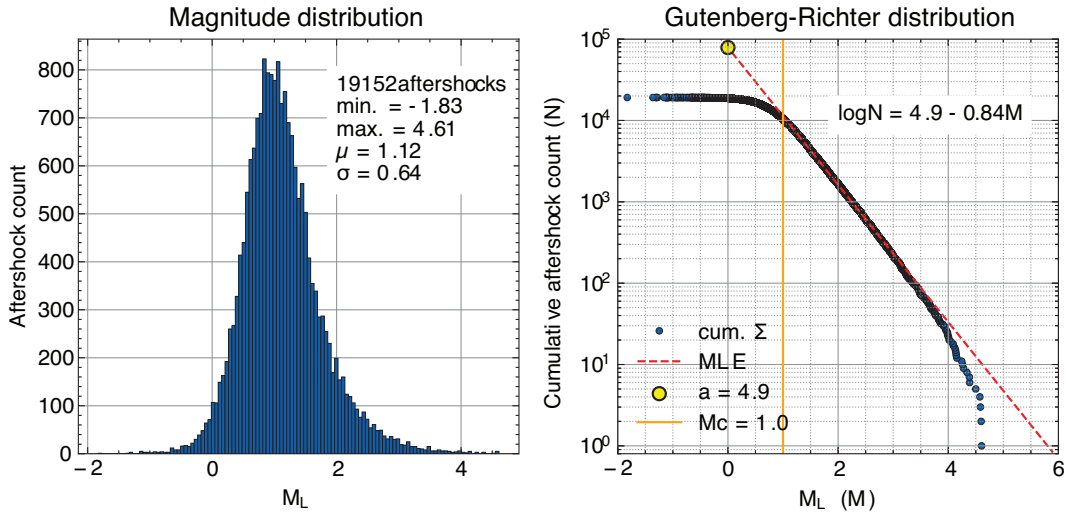

Figure 5. The magnitude distribution (left panel) and cumulative frequency–magnitude distribution with Gutenberg–Richter fit (right panel) for the relocated ML-based aftershock catalogue. Earthquake magnitudes were calculated using the empirical local magnitude relationship of B. Muço & P. Minga (1991).

Subsequently, the earthquake catalogue was relocated using the new velocity model and station corrections (Fig. S2, Supplementary Information). With these updates, the median absolute errors estimated by NLL decreased from 4.0 to 2.3 km in the x-direction, from 3.4 to 1.6 km in the y-direction and from 4.3 to 2.7 km in depth (Fig. S3, Supplementary Information).

Magnitude determination

Local magnitudes (Ml) were calculated using an empirical attenuation relationship for Albania (B. Muço & P. Minga 1991). The resulting catalogue spans magnitudes from −1.83 to 4.61 (Fig. 5). The frequency–magnitude distribution follows the Gutenberg–Richter relation; maximum-likelihood fitting yields an a-value of 4.9 and a b-value of 0.84. The catalogue is complete above Mc $\approx$ 1.0. The relatively low b-value (<1) suggests a proportionally higher occurrence of larger aftershocks relative to smaller ones.

HypoDD relocation

We used the double-difference algorithm (F. Waldhauser & W.L. Ellsworth 2000) to further refine the locations. We calculated differential traveltimes based on waveform cross-correlation within time windows spanning 0.3 s before to 0.7 s after P- and S-phase arrivals on the vertical and the two horizontal components, respectively. We integrated the horizontal traces containing the S-phase to displacement prior to cross-correlation, as this was found to enhance the S-phase signal. A 3-pole causal 1–10 Hz Butterworth band-pass filter was applied to all waveforms. We calculated the cross-correlation function for event pairs with a maximum hypocentral separation of 7 km based on the joint hypocentre locations. For the S-phase windows, we stacked the cross-correlation function of the two horizontal components and obtained the lag time and correlation coefficient from the maximum amplitude of the stack. Lag times with a correlation coefficient > 0.7 were kept and furnished with the correlation coefficient as a weight for the hypocentre inversion. This procedure yielded 934 204 lag time measurements. The relocations were done using the new 1-D velocity model. HypoDD omits events that are not well enough linked, reducing the total number of relocated events. In addition, we excluded events with no observations within an epicentral distance of 15 km, resulting in a final catalogue of 13 251 events (Fig. 6). The hypoDD relocation sharpens structures in cross-section significantly when comparing with the joint hypocentre determination locations (Fig. S2, Supplementary Information).

RESULTS

The first events were detected 17 d after the mainshock. Although the most vigorous period of aftershock activity was not recorded, seismicity remained high during the initial weeks of network operation. Over the nine months of observation, the weekly number of aftershocks declined steadily, from approximately 1500 earthquakes in December 2019 to five in September 2020. Generally, the network deteriorated over its operation lifetime causing a decline of the magnitude of completeness (Mc) from 0.6 in December 2019 to 1.5 in July 2020 and 2.2 afterwards (Fig. 7). The general decrease in aftershock seismicity is punctuated by six Ml 4 + aftershock subsequences, indicated by different colours in Figs 6–8.

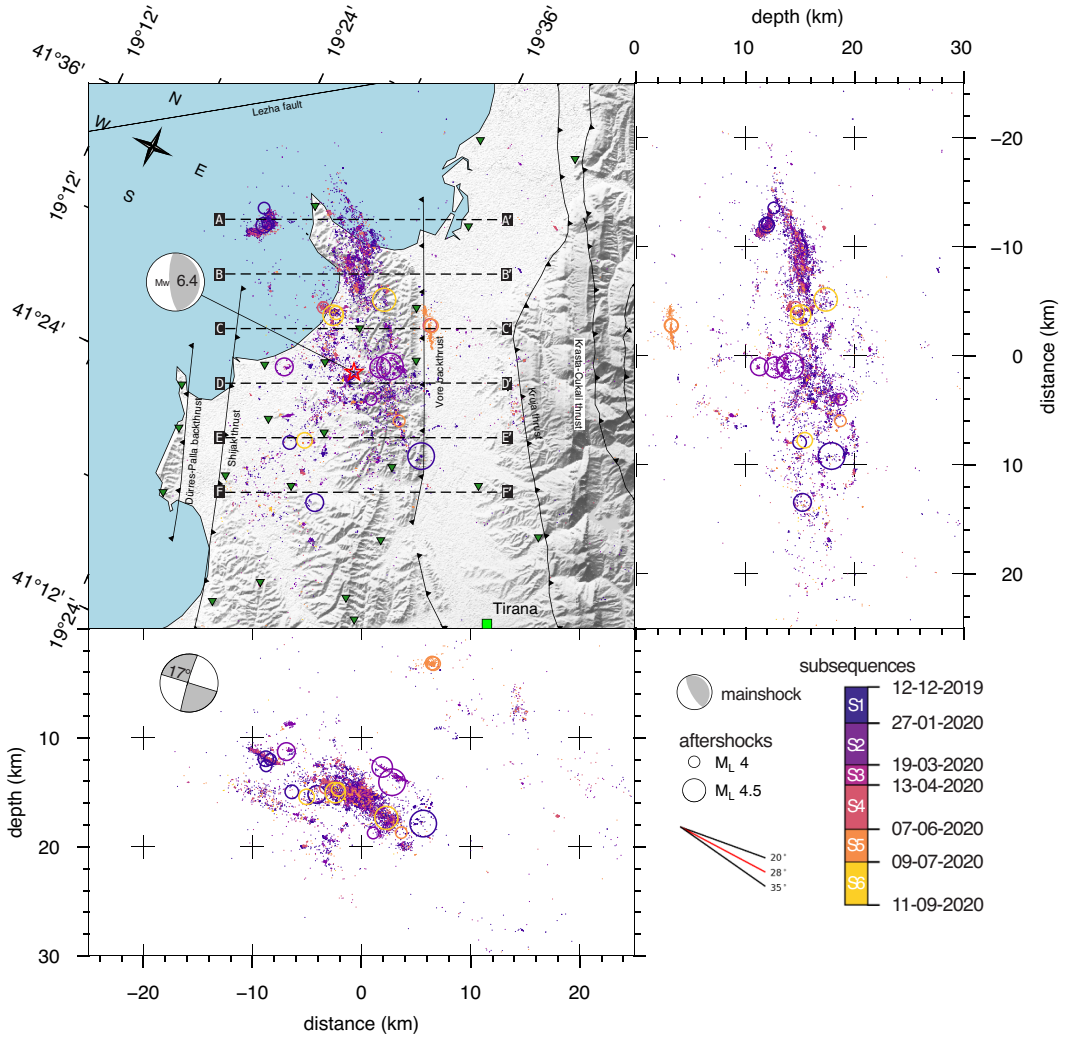

Figure 6. 13 251 relocated hypocentres obtained using double-difference algorithm (F. Waldhauser & W.L. Ellsworth 2000) in map view (rotated by 25° azimuth) and in two vertical cross-sections along the extent of the two map directions (distance in km is from the centre of the map). Hypocentres are coloured according to aftershock subsequence (see also Fig. 7). The stippled lines marked A–F locate the vertical profiles depicted in Fig. 8.

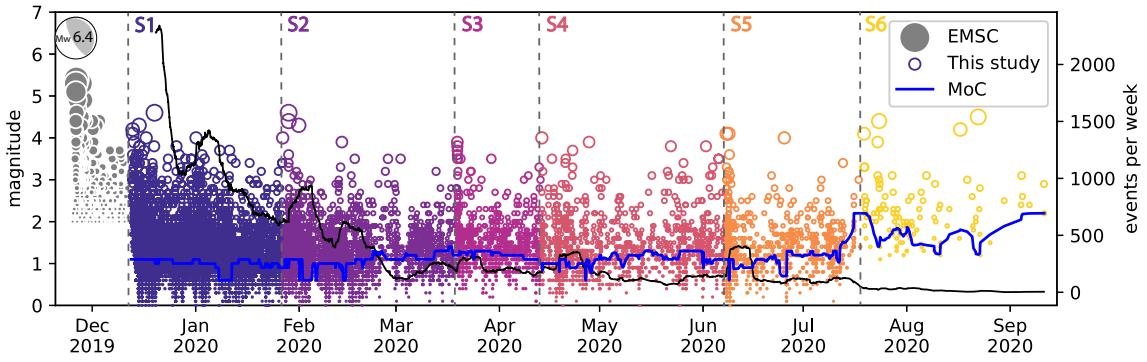

Figure 7. Magnitude versus time for the 2019 M_w 6.4 Durrës aftershock sequence. Magnitudes (M_w) of the Durrës mainshock and first two weeks of aftershocks (Ml) are taken from the EMSC catalogue (grey circles). For the period covered by our network, local magnitudes (Ml) are plotted. Colours divide different subsequences initiated by larger Ml4 + aftershocks. The blue line marks the time-dependent magnitude of completeness (MoC), and the black line marks the number of events in the preceding week.

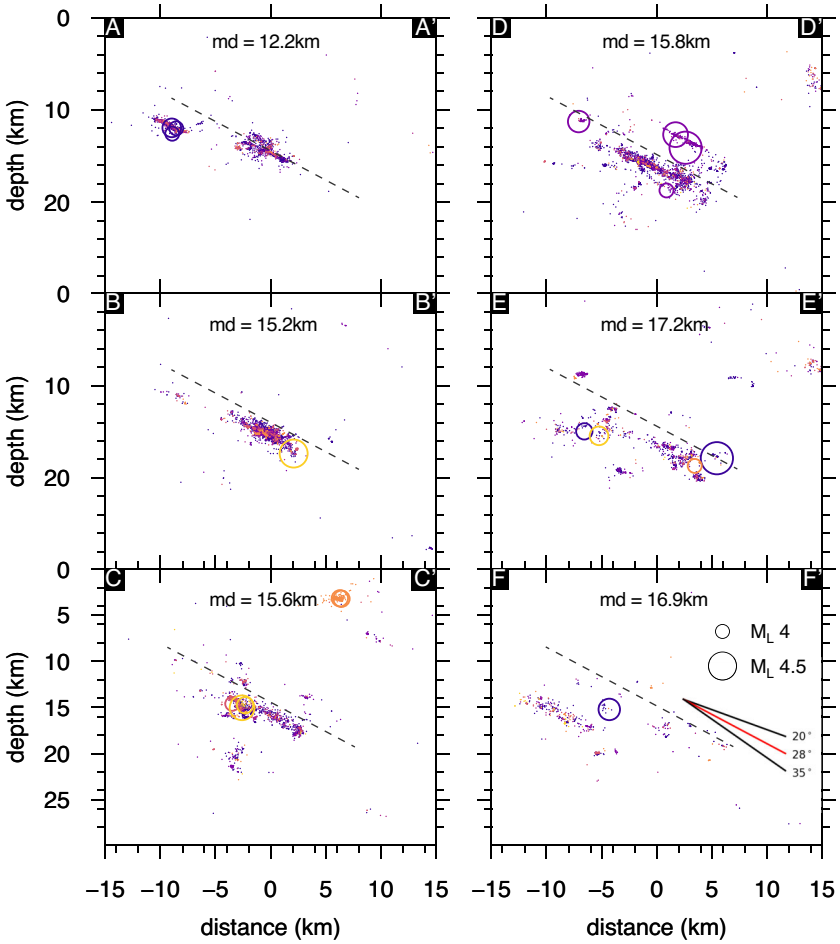

Figure 8. Hypocentre cross-sections sorted from north (A) to south (F) along the projection lines indicated in Fig. 6. Hypocentres are coloured according to aftershock subsequence (see also Fig. 7). The dashed line, representing a 28° dip, is maintained at the same position in all cross-sections to illustrate the gradual deepening of the main fault structure towards the south. md is the median depth of the plotted seismicity.

The aftershock seismicity is strongly clustered over a 20 by 30 km region in map view, covering a depth range between 2 and 22 km (Fig. 6). All aftershocks are located between the Shijak frontal- and Vore back-thrust (Fig. 6) showing a large onshore cluster and a smaller, but dense offshore cluster. Seismicity in the onshore cluster is distributed along NW–SE oriented lineaments, which generally slightly deepen towards the SE (see along-strike vertical cross-section on right side of Fig. 6). An eastward deepening of the general seismicity is observed, (see cross-sections in Figs 7 and 8). The median depth increases from 12.2 to 16.9 km from northwest to southeast (Figs 8A–F). The shallow offshore cluster is associated with three Ml4 + aftershocks, delineating a thin horizon of at most 1 km wide in cross-section, dipping towards northeast (Fig. 8A). Separated by a 4 km-wide lateral seismic gap, the deeper onshore cluster has a similar dip and is surrounded by minor, scattered seismicity above and below. 5 km further southeast (Fig. 8B), the onshore cluster retains its dip-angle but thickens to a 2 km-thick horizon. Even though the Ml 4 + aftershock in Fig. 8(B) is associated with the major onshore cluster, no microseismicity was recorded as the service of the seismic network was ending mid-July 2020 (Fig. 7).

The major onshore cluster is continuously observed for 10 km along-strike further southeast (Fig. 8D) where it spans an 8 km-wide region at depth. Moreover, a parallel horizon of seismicity associated with two Ml 4 + aftershocks is observed 5 km above the major onshore cluster. Seismicity further southeast (Figs 8E and F) shows numerous small but dense aftershock clusters collectively forming a northeast dipping trend. Cross-section F (Fig. 8 F) shows another NE dipping cluster; this is not a continuation of the main structure, but another, subparallel and deeper cluster. A very shallow burst of seismicity is observed (Fig. 8C) at the beginning of June 2020 (subsequence Vore) activating a line of seismicity at ∼3.5 km depth, associated with two Ml 4 + aftershocks.

DISCUSSION

The relation between aftershocks and mainshock slip

Our study demonstrates that relatively simple, inexpensive experiments using easy-to-deploy geophones, combined with modern ML-based analysis, are highly effective, particularly for post-seismic campaigns targeting high-rate aftershock sequences. Analysing such a

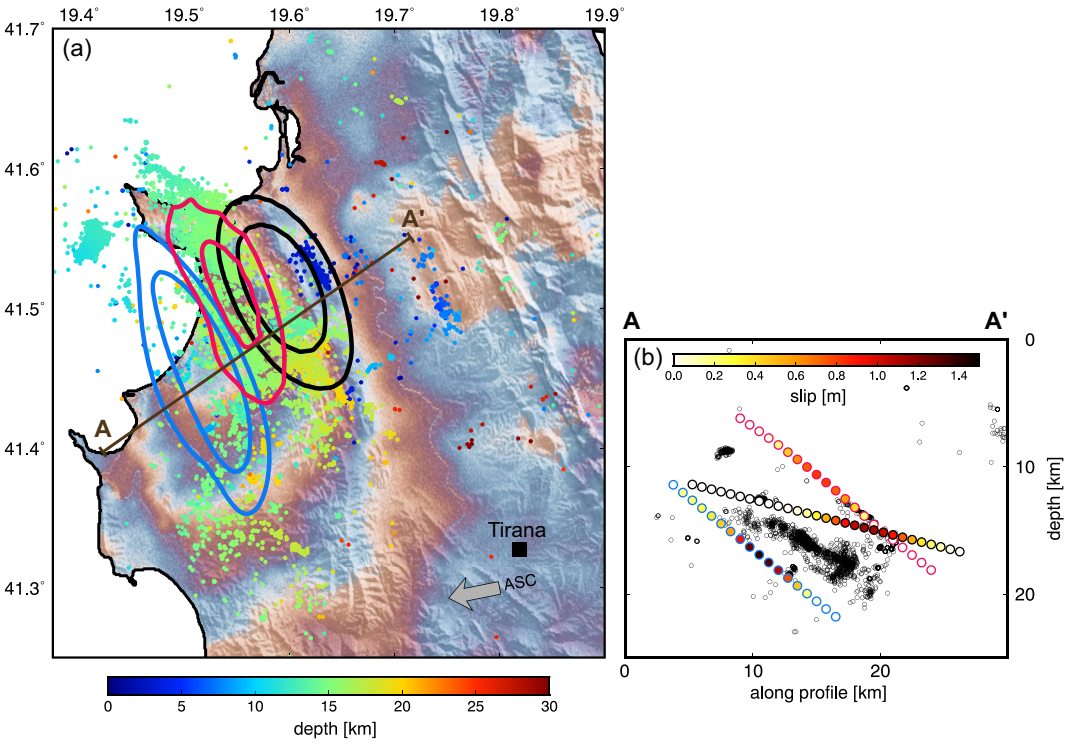

Figure 9. (a) Depth colour-coded aftershocks plotted over the interferogram of ascending track of the Sentinel 1 satellite draped over topography. Slip isolines of 0.35 and 0.7 m are shown for the slip models on the NE dipping plane of K. Matraku *et al.* (2023) (blue), M. Govorčin *et al.* (2020) (black) and H. Panuntun (2021) (red). Line locates the cross-section in panel (b). The arrow points to ascending look direction of the satellite. (b) Central cross-section of 5 km swath through seismicity and the three slip models. Circle colour is the same as slip lines in panel (a). Circle filling is the slip magnitude for the cross-section.

large number of events in a traditional way with visual phase picking would have been hardly feasible. Only dense seismicity volumes, however, make visualization of faint seismic structures and their detailed interpretation possible.

Our results show clearly that the rupture occurred on a NE-dipping plane with several subparallel structures activated post-seismically, as well as shallow rupture near the Vore backthrust initiated with three M4 + aftershocks late in the sequence. Although the ambiguity of the fault plane is solved by our data, the location of the main rupture remains uncertain, as the densest aftershock cluster may not correspond to the main slip region (S. Das & C. Henry 2003). Aftershocks often cluster at the margins of slip maxima, where stresses were increased (e.g. C.-H. Chang *et al.* 2007; C.-H. Chan & R.S. Stein 2009).

Several slip models have been published, but in absence of near-source seismic data, they rely mainly on interferometric synthetic aperture radar (InSAR) and sparse Global Navigation Satellite System (GNSS) data. We plot three of them in Fig. 9 in map view and cross-section. For the model of M. Govorčin *et al.* (2020) we chose the slip distribution on the NE dipping plane. They all show a similar elliptic slip zone, yet shifted, placing the aftershock cluster either updip of (M. Govorčin *et al.* 2020), congruent to (H. Panuntun 2021) or downdip of (K. Matraku *et al.* 2023) the main slip patch. This ambiguity presumably stems from the uncertainty of the chosen fault plane geometry, that is, depth and dip, for which the slip inversions were performed (Fig. 9b). M. Govorčin *et al.* (2020) and K. Matraku *et al.* (2023) searched for an optimized geometry and found a depth of ∼15 km and a dip of 15° and a depth of 18 km and 40° dip, respectively. H. Panuntun (2021) simulated a listric fault with dips from 30° to 44° but highest slip was found at 10 km depth where the fault plane had a 40° dip. Both dip and depth seem not well constrained in these models, when compared among them and with the fault plane from aftershocks (Fig. 9b). Our findings, that is, a centroid depth of the main cluster of ∼15 km and a dip of ∼28° is not correctly picked up by any of the models (Fig. 9b). Given the pronounced contrast between the basement and the overlying sediment stack, as revealed by our velocity inversion, the common assumption of a half-space structure in elastic modelling may introduce additional error in the location of slip. It may hence be justified to now develop a better-informed model based on better constrained fault plane geometry and medium properties; however, this is beyond the scope of this study.

Most centroid depths from moment tensor inversions of the mainshock are significantly deeper than the aftershock cluster (Table 1; ∼20–26 km). This may indicate that the main slip occurred downdip of the aftershocks, which cluster near its updip termination (Fig. 10). Alternatively, the discrepancy could result from inaccuracies in the structural model used for the Green's Functions. For example, neglecting the low-velocity sediments above the source can lead to an overestimation of the centroid depth, as the surface reflection that constrains depth for body waves is implicitly modelled. Similar effects may come into play for more complex regional wavefields. Our results highlight the large uncertainties in basic source parameters determined using well-established methods for a European earthquake when limited near-source data are available.

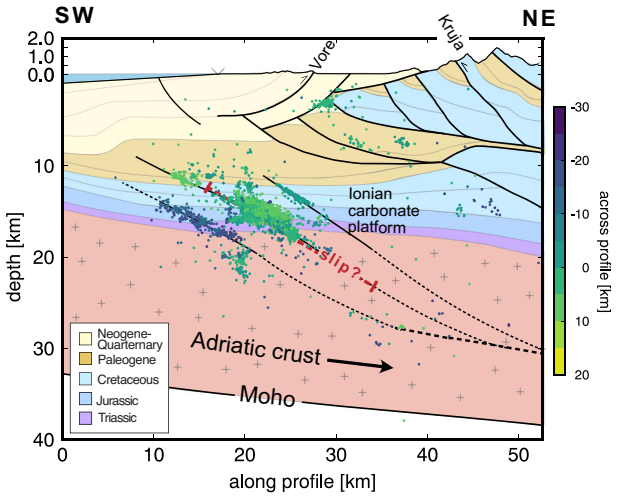

Figure 10. Structural cross-section based on F. Roure *et al.* (2004). The location of the seismicity centre profile is shown in Fig. 2; zero distance is at the SW start of the profile. Aftershocks are colour coded according to across profile distance; zero distance is at the profile location. Aftershocks delineate several subparallel, NE dipping planes interpreted as splay faults. Thrusts are blind, lying beneath Neogene sediments and cutting through a carbonate platform, possibly extending into the Adriatic basement. Red dashed line illustrates the uncertain location of the mainshock slip. The black dashed lines indicate a hypothesized detachment interface within the Adriatic crust and possible splay faults. See Discussion.

LINKING THE DURRËS EARTHQUAKE TO REGIONAL TECTONICS

We can now place our results in the structural context of the fold and thrust belt at the tip of the internal Albanides. The region's upper crust has been partially illuminated by seismic and borehole studies investigating its hydrocarbon potential (e.g. F. Roure *et al.* 2004; A. Frasheri *et al.* 2009), providing a basis for constructing structural profiles. The geological map of Albania (A. Xhomo *et al.* 2002) is also accompanied by a set of cross-sections; two of them pass our aftershock region along its northern (profile III) and southern boundary (profile IV) in A. Xhomo *et al.* (2002). The profile published by F. Roure et al. (2004) is almost coincident with profile IV of A. Xhomo *et al.* (2002). Resolution of these sections is limited to the upper ∼10 km of the crust. As others have done (e.g. S. Teloni *et al.* 2020; E. Vittori *et al.* 2021), we guide our interpretation by the profile published by F. Roure et al. (2004), but also consider the profiles of A. Xhomo *et al.* (2002). We plot a cross-section through the aftershock zone parallel to Roure's section (Fig. 10, see Fig. 2 for location) and fix it in the NE at the outcrop of the Kruja Nappe.

The section shows the duplex structure of Cretaceous to Paleogene carbonates in the NE and Neogene basin in the SW. The contrast between the seismically fast carbonates in the NW and seismically slow sediments above and to the SW of the aftershock zone is probably responsible for the systematic variation of station corrections observed in the traveltime inversion (Fig. 4). Profile III of A. Xhomo *et al.* (2002) shows a monocline of folded sediments in the SW, which we adopt and interpret as potentially resulting from the tip of the blind thrust responsible for the Durrës earthquake. The seismicity not related to the NE dipping thrust system is contained mostly in the duplex structure of the hanging wall and possibly along the bounding roof thrust. These events demonstrate that shallow secondary faults may become seismically active in relation with movement on the deeper thrust. Although the events were moderate (∼M4), the possibility of larger events cannot be ruled out and their very shallow depth poses a significant hazard to, for example, Tirana, which sits on top of a hanging wall duplex structure.

The NE dipping thrust system itself lies beneath the Neogene sediments and all subparallel thrusts break through the Ioanian (Triassic–Jurassic) carbonate platform sequence and possibly into the basement (depending on where mainshock slip was located relative to the aftershocks), that is, into relatively deep competent rocks (Fig. 10). The Ionian platform top appears clearly as a paleoslope in the published reflection data (F. Roure *et al.* 2004) and should therefore be relatively well resolved. The observed thrust dips from the aftershock distribution (∼30°) are inconsistent with reactivation of steeper normal faults known to cut through the Apulian continental margin and are therefore likely newly formed. The Durrës earthquake sequence may reflect the formation of a ramp accommodating the displacement of a new thrust sheet of Ionian provenance.

Triassic evaporites, which typically act as an efficient detachment facilitating thin-skinned shortening of the Ionian basin in central Albania, appear to be absent in our study region (F. Roure *et al.* 2004; S. Teloni *et al.* 2020). We therefore root the sequence of thrusts speculatively in a mid-crustal detachment as suggested also by S. Teloni *et al.* (2020). Some of the deepest aftershocks at ∼25 km depth could be vaguely indicative of such a structure (Fig. 10). A. Copley *et al.* (2009) proposed that the thick sedimentary cover of the Albanian lowlands could enhance heating of the basement through thermal blanketing and radiogenic heat production, thereby facilitating the development of a ductile weak zone within the crust. In such a scenario, the Durrës earthquake sequence would represent active splay faulting branching from a mid-crustal detachment zone at the tip of a continental subduction system.

The structure sketched in Fig. 10 further implies that part of the Adriatic middle crust is detached and underplated beneath the upper plate, contributing to crustal thickening. This has been proposed by B.C. Burchfiel *et al*. (2018) as a key mechanism constructing the crust of the Hellenides in particular and for retreating subduction systems in general. Large-scale mid-crustal slicing and underplating has also been invoked by F. Rossetti et al. (2024) to explain 3–4 km of exhumation during the latest Miocene–Pliocene in southernmost Albanides. A separation of the Adriatic crust along a decollement would facilitate its partial subduction by reducing buoyancy forces. The continental Adriatic plate has been subducted in tow of the Vardar Ocean since ∼150 Ma and deep subduction of the Adriatic plate is revealed by a NE dipping high-velocity zone down to 150 km depth in the mantle beneath the Albanides (C. Piromallo & A. Morelli 2003; M.R. Handy *et al*. 2019). However, subducting an intact ∼30 km thick crust to this depth would be difficult due its low density.

CONCLUSIONS

This study provides a comprehensive analysis of the M_w 6.4 Durrës earthquake aftershock sequence, revealing the underlying tectonic and structural framework. Based on a dense temporary local seismic network and utilizing modern machine learning methods, we were able to detect ∼19k events and relocate about ∼13k events with high precision, illuminating the fault structures activated during this seismic event. Local magnitudes range between −1.83 and 4.6 with a magnitude of completeness of about 1. We find a *b*-value of the Gutenberg–Richter distribution of 0.84 for the aftershock sequence. Based on measured traveltimes, we inverted for a new 1-D velocity model and accompanying station corrections for *P*- and *S*-waves. The velocity model shows strong depth variability for *P* and *S*, accounting for a thick sedimentary layer over the Adriatic crystalline basement. A systematic change from positive station correction terms in the SW to negative station correction terms in the NE likely reflects the juxtaposition of thrusted and stacked fast carbonate rocks of the Kruja zone to slow Neogene and Quaternary sediments in the SW. The aftershocks are concentrated between the Shijak frontal thrust and Vore back-thrust, with distinct onshore and offshore clusters. They reveal in cross-section several sharp, subparallel NE dipping planes, with the most prominent one probably responsible for the mainshock. This plane ranges between ∼12 and 18 km depth and dips ∼28° to the NE; it tilts slightly towards the SE. Given the structural context from seismic lines and geological maps, all NE dipping faults are clearly located beneath the thick Neogene sediments and cut through carbonate platform rocks and into the Adriatic plate crystalline basement. The Durrës earthquake hence exhibits basement-involved, thick-skinned faulting and suggests ongoing large-scale slicing and underplating of subducted Adriatic crust. A sequence of three M4+ and their aftershocks was observed six months after the mainshock at a shallow depth ∼3.5 km depth, in the hanging wall. This sequence highlights the potential hazard posed by shallow secondary faults in the region.

ACKNOWLEDGMENTS

The initial field campaign was funded by GFZ' Hazard and Risk Team (HART) programme. Instruments were provided by the Geophysical Instrument Pool Potsdam (GIPP). We thank the whole IGEO for support in the field. We used ObsPy (L. Krischer *et al*. 2015) and SeisBench (J. Woollam 2022) for parts of the data analysis and GMT (P. Wessel *et al*. 2019) for plotting. We acknowledge helpful discussions with Mark Handy and Silvia Crosetto. Sabrina Metzger helped creating Fig. 9.

SUPPORTING INFORMATION

Supplementary data are available at *GJIRAS* online.

Figure S1. Detected event hypocentres located using a published velocity model for entire Albania (R. Ormeni, 2011). Hypocentres are coloured according to aftershock subsequence (see also Fig. 6). Map is rotated by 25° with respect to North direction. Vertical cross-sections along the extent of the two map directions (distance in km is from the centre of the map).

Figure S2. 19.152 hypocentres after relocation with the new 1-D velocity model and corresponding station correction terms. Hypocentres are coloured and categorized after aftershock subsequences. Map rotated by 25°. Mainshock epicentre from GFZ.

Figure S3. Absolute location (*x*, *y*, *z*) errors in kilometres after location with the velocity model currently available for Albania (initial; R. Ormeni, 2011) and the new 1-D velocity model (relocated).

Table S1. Tabulated 1-D velocity model for the Durrës earthquake region from travel time inversion.

Table S2. *P*-wave and *S*-wave station corrections corresponding to the updated 1-D velocity model (Table S1, Supplementary Information).

Please note: Oxford University Press are not responsible for the content or functionality of any supporting materials supplied by the authors. Any queries (other than missing material) should be directed to the corresponding author for the article.

DATA AVAILABILITY

The seismic waveform data used in this study is openly available from the GEOFON data centre (https://geofon.gfz.de/waveform) under the network code 9 K, 2019–2020 (B. Schurr *et al*. 2020). The relocated earthquake catalogue is available from B. Schurr *et al*. (2026).

REFERENCES

Benetatos, C. & Kiratzi, A., 2006. Finite-fault slip models for the 15 April 1979 (Mw 7.1) Montenegro earthquake and its strongest aftershock of 24 May 1979, (Mw 6.2). *Tectonophysics,* **421**(1–2), 129–143.

Burchfiel, B.C., Royden, L.H., Papanikolaou, D. & Pearce, F.D., 2018. Crustal development within a retreating subduction system: the Hellenides, *Geosphere,* **14**(3), 1119–1130.

Chan, C.-H. & Stein, R.S., 2009. Stress evolution following the 1999 Chi-Chi, Taiwan, earthquake: consequences for afterslip, relaxation, aftershocks and departures from Omori decay, *Geophys. J. Int.,* **177**(1), 179–192.

Chang, C.-H., Wu, Y.-M., Zhao, L. & Wu, F.T. , 2007. Aftershocks of the 1999 Chi-Chi, Taiwan, earthquake: the first hour, *Bull. seism. Soc. Am.,* **97**(4), 1245–1258.

Copley, A., Boait, F., Hollingsworth, J., Jackson, J. & McKenzie, D., 2009. Subparallel thrust and normal faulting in Albania and the roles of gravitational potential energy and rheology contrasts in mountain belts, *J. Geophys. Res.: Solid Earth,* **114**(5).

D'Agostino, N. *et al.*, 2020. Active crustal deformation and rotations in the southwestern Balkans from continuous GPS measurements, *Earth planet. Sci. Lett.,* **539,** 116246.

Das, S. & Henry, C., 2003. Spatial relation between main earthquake slip and its aftershock distribution, *Rev. Geophys.,* **41**(3).

Frasheri, A., Bushati, S. & Bare, V., 2009. Geophysical outlook on structure of the Albanides, *J. Balkan Geophys. Soc.,* **12,** 9–30.

Freddi, F., Novelli, V., Gentile, R., Veliu, E., Andreev, S., Andonov, A. Greco, F. & Zhuleku , E., 2021. Observations from the 26th November 2019 Albania earthquake: the earthquake engineering field investigation team (EEFIT) mission, *Bull. Earthquake Eng.,* **19**(5), 2013–2044.

Ganas, A., Elias, P., Briole, P., Cannavo, F., Valkaniotis, S., Tsironi, V. & Partheniou, E.I., 2020. Ground deformation and seismic fault model of the M6.4 Durres (Albania) nov. 26, 2019 earthquake, based on GNSS/INSAR observations, *Geosciences (Switzerland),* **10**(6), 1–16.

Govorčin, M., Wdowinski, S., Matoš, B. & Funning, G.J., 2020. Geodetic source modeling of the 2019 Mw 6.3 Durrës, Albania, earthquake: partial rupture of a blind reverse fault, *Geophys. Res. Lett.,* **47**(22). e2020GL088990.

Handy, M.R., Giese, J., Schmid, S.M., Pleuger, J., Spakman, W., Onuzi, K. & Ustaszewski, K., 2019. Coupled crust-mantle response to slab tearing, bending, and rollback along the dinaride-hellenide orogen, *Tectonics,* **38**(8), 2803–2828.

Handy, M.R., Ustaszewski, K. & Kissling, E., 2015. Reconstructing the Alps–Carpathians–Dinarides as a key to understanding switches in subduction polarity, slab gaps and surface motion, *Int. J. Earth Sci.,* **104,** 1–26

Jouanne, F. *et al.*, 2012. GPS constraints on current tectonics of Albania, *Tectonophysics,* **554–557,** 50–62.

Kissling, E., Ellsworth, W.L., Eberhart-Phillips, D. & Kradolfer, U., 1994. Initial reference models in local earthquake tomography, *J. Geophys. Res.: Solid Earth,* **99**(B10), 19 635–19 646.

Krischer, L., Megies, T., Barsch, R., Beyreuther, M., Lecocq, T., Caudron, C. & Wassermann, J., 2015. ObsPy: a bridge for seismology into the scientific Python ecosystem, *Comput. Sci. Discovery,* **8**(1), 014 003.

Lomax, A., Virieux, J., Volant, P. & Berge-Thierry, C., 2000. Probabilistic earthquake location in 3D and layered models, *Advances in Seismic Event Location,* pp. 101–134, Springer-Verlag.

Markušić, S., Ivančić, I. & Sović, I., 2017. The 1667 Dubrovnik earthquake–some new insights, *Stud. Geophys. Geod.,* **61**(3), 587–600.

Matraku, K., Jouanne, F., Dushi, E., Koçi, R., Kuka, N., Grandin, R. & Bascou, P., 2023. The 26 November 2019 Durrës earthquake, Albania: coseismic displacements and occurrence of slow slip events in the year following the earthquake, *Geophys. J. Int.,* **234**(2), 807–838.

Muço, B. & Minga, P., 1991. Magnitude determination of near earthquakes for the Albanian network, *Bollettino Di Geofisica Teorica EdApplicata,* **33**(129), 17–24.

Ormeni, R., 2011. P, S wave velocity model of the crust and upper most mantle of Albania region, *Tectonophysics,* **497**(1–4), 114–121.

Panuntun, H. , 2021. Geodetic slip model of the November 26, 2019 Albania earthquake estimated from Sentinel-1 TOPS interferometry, *Tectonophysics,* **807,** 228 814.

Pezzo, G., Palano, M. & Chiarabba, C., 2022. Rotation at subduction margins: how complexity at fault-scale (the 2019 Albanian Mw 6.4 earthquake) mirrors the regional deformation, *Terra Nova,* **34**(3), 244–252.

Piromallo, C. & Morelli, A., 2003. P wave tomography of the mantle under the Alpine-Mediterranean area, *J. Geophys. Res.: Solid Earth,* **108**(B2). 2065.

Rossetti, F. *et al.*, 2024. Building the Albanides by deep underplating, *Tectonics,* **43**(11), 43. e2024TC008506.

Roure, F., Nazaj, S., Mushka, K., Fili, I., Cadet, J.-P. & Bonneau, M., 2004. Kinematic evolution and petroleum systems—an appraisal of the outer albanides, *AAPG Mem.,* **31**(82), 881–913.

Schurr, B., Dushi, E., Rietbrock, A. & Duni, L., 2020. AlbACa—Albanian earthquake aftershock campaign, *GFZ Data Services, Dataset/Seismic Network*.

Schurr, B., van der Heiden, V., Woollam, J., Dushi, E., Tilmann, F. & Rietbrock, A. , 2026. Aftershock catalogue for the 2019 M6.4 Durrës, Albania earthquake, *GFZ Data Services,*

Tan, Y.J. *et al.*, 2021. Machine-learning-based high-resolution earthquake catalog reveals how complex fault structures were activated during the 2016–2017 Central Italy sequence, *Seismic Record,* **1**(1), 11–19.

Teloni, S., Invernizzi, C., Mazzoli, S., Pierantoni, P.P. & Spina, V., 2020. Seismogenic fault system of the Mw 6.4 November 2019 Albania earthquake: new insights into the structural architecture and active tectonic setting of the outer Albanides, *J. Geol. Soc.,* **178**(2).

Vittori, E., Blumetti, A.M., Comerci, V., Di Manna, P., Piccardi, L., Gega, D. & Hoxha, I., 2021. Geological effects and tectonic environment of the 26 November 2019, Mw6.4 Durres earthquake (Albania), *Geophys. J. Int.,* **225**(2), 1174–1191.

Waldhauser, F. & Ellsworth, W.L., 2000. A double-difference earthquake location algorithm: method and application to the Northern Hayward Fault, California, *Bull. seism. Soc. Am.,* **90**(6), 1353–1368.

Wessel, P., Luis, J.F., Uieda, L., Scharroo, R., Wobbe, F., Smith, W.H.F. & Tian, D., 2019. The generic mapping tools version 6, *Geochem. Geophys. Geosyst.,* **20**(11), 5556–5564.

Woollam, J. *et al.*, 2022. SeisBench—A toolbox for machine learning in seismology, *Seismol. Res. Lett.,* **93**(3), 1695–1709.
Woollam, J., Rietbrock, A., Leitloff, J. & Hinz, S., 2020. HEX: hyperbolic event eXtractor, a seismic phase associator for highly active seismic regions, *Seismol. Res. Lett.,* **91**(5), 2769–2778.
Woollam, J., Van der Heiden, V., Rietbrock, A., Schurr, B., Tilmann, F. & Dushi, E., 2022. Machine learning event detection workflows in practice: a case study from the 2019 Durrës aftershock sequence, ArXiv E-Prints. Retrieved from https://ui.adsabs.harvard.edu/abs/2022arXiv220512033W
Xhomo, A. *et al.*, 2002. *Geological Map of Albania*. scale 1:200,000, published by the Ministry of Industry and Energy, Republic of Albania.
Zhu, W. & Beroza, G.C., 2019. PhaseNet: a deep-neural-network-based seismic arrival-time picking method, *Geophys. J. Int.,* **216**(1), 261–273.